Interface erosion sensibility of cohesive fine soils

Didier Marot, Hong Haï Nguyen, Fateh Bendahmane, Ouali Amiri, Stéphanie Bonnet

Interface erosion sensibility of cohesive fine soils

D. Marot[1], H.H. Nguyen[2], F. Bendahmane[1], O. Amiri[1], S. Bonnet[1]

[1]*Institut GeM, University of Nantes – ECN – CNRS, BP 420, 44606 Saint-Nazaire Cedex, France*

[2]*University of Science and Technology, Danang, Vietnam*

Corresponding author: D. Marot (e-mail: didier.marot@univ-nantes.fr).

ABSTRACT: Erosion is one of the main causes of instabilities within hydraulic earth structures as dams, dikes or levees. This paper deals with the interface erosion phenomenon between soil and water, and the Jet Erosion Test is used in order to evaluate the erodibility of two types of clayey sand. Twenty three specimens are compacted using a normal Proctor technique and results are analyzed with energy based method and also with Hanson and Simon's method. Energy based method is less conservative and appears more efficient in order to elaborate a relative classification of erodible soils. For both types of clayey sand, the erosion sensibility, defined by the erosion resistance index is linearly related with saturation ratio. The parametric study also highlights the influence on the interface erosion sensibility of the micro fabric of tested soils.

1 INTRODUCTION

1.1 *Terminology and context*

Under internal seepage flow, hydraulic earth structures (such as dikes, levees, or dams and their foundations) can incur an erosion of some particles of their constitutive soil. Two types of internal erosion processes can be distinguished: suffusion and interface erosion. Suffusion process concerns only the finer particles which are detached and then move inside the soil matrix which is composed of coarse particles. Interface erosion can appear in cracks or concentrated leaks and is then called piping (Fell & Fry, 2007). When the interface erosion appears between two materials having different grain size distributions, it is called contact erosion. However this interface, relatively large compared to the grain scale, can also be located between soil and water. In such case and with a seepage flow which is normal to the interface, process is called backward erosion.

Interface erosion is one of the main phenomena in earth structures and their foundations which may increase their failure risk. With the objective to contribute to the safety assessment of these earth structures, various researchers developed different testing devices for characterizing the sensibility of interface erosion of fine soils. Among these testing devices, the Jet Erosion Test (JET) is commonly used because it can simplify studies on low plasticity soils or on saturated soils. Another advantage of the JET is that it can be used on site and measure the intact resistance.

1.2 *Principle of Jet Erosion Test*

The JET was developed by Dunn (1959) and had been further improved by Hanson and Cook (2004). This apparatus is designed to apply a submerged water jet on the face of a soil specimen. Such an apparatus is described in the A.S.T.M. Standard D5852. In laboratory, soil specimens are compacted in a standard Proctor mold.

Figure 1 shows the principles of the device. The jet test apparatus consists of an adjustable head tank, a jet tube with a nozzle, a point gage and a jet submerged tank which contains the specimen.

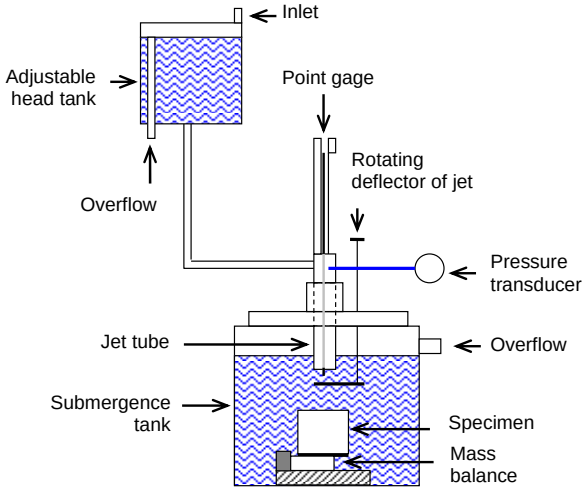

Figure 1. Schematic diagram of the Jet Erosion Test device.

The point gage is adjusted to close off the nozzle and also to measure, at increasing time intervals the depth of scour (J) beneath the nozzle (d_0 diameter).

The device used for this study comprises also a mass balance which is placed under the specimen in order to measure the variations of specimen mass for the experiment duration.

1.3 *Interpretative methods and soil erodibility classifications*

Two existing interpretative methods for JET apparatus can be distinguished.

The first method which is proposed by Hanson & Simon (2001) is based on a linear erosion law which relates the volumetric rate of erosion, $\dot{\varepsilon}$, to the excess hydraulic shear stress τ above a threshold value τ_c. This threshold of hydraulic shear stress represents the minimal value needed to initiate erosion. In equation form, the erosion laws are:

$$\dot{\varepsilon} = k_d \left(\tau - \tau_C\right) \tag{1}$$

where k_d is the erosion rate coefficient.

At t=0, the initial distance to the interface is written as J_0. At an infinite time, J tends to a limit, the equilibrium depth J_e. For distances smaller than J_p=6.2 d_0, the flow consists of a potential core in which the velocity is equal to the initial velocity u(0,0) at the jet origin, and an outer zone where the axial velocity varies inversely with the distance:

$$u(0,\ J) = \frac{J_p}{J}\, u(0,0) \tag{2}$$

The equivalent hydraulic shear stress applied to the soil surface can be computed in function of the water velocity u(0,J) on the centerline of the jet:

$$\tau = C_f\ \rho\ u(0,J)^2 \tag{3}$$

where C_f is the friction coefficient which is assumed to be constant, C_f = 0.00416.

The erosion law is not dimensionalized and a characteristic time is defined. By integrating the no dimensional erosion law, time is expressed as a function of no dimensional depth J*.

$$t = T_R\left(-J^*\Big|_{J_i^*}^{J^*} + \frac{1}{2}\,\mathrm{Ln}\left(\frac{1+J^*}{1-J^*}\right)\Big|_{J_i^*}^{J^*}\right) \tag{4}$$

$$\text{with } T_R = \frac{J_e}{k_d.\tau_C} \tag{5}$$

$$\text{and } J^* = \frac{J}{J_e} \tag{6}$$

The evolution of the scour depth with time is fitted to a hyperbolic function that predicts the ultimate depth of scour, equivalent to the equilibrium depth (Blaisdell & Anderson, 1981). It leads to the determination of the critical shear stress τ_C. The experimental data is fitted to the model represented by Equation (6). This yields an estimate of the characteristic time and the resulting detachment rate coefficient, k_d, which is expressed on a volumetric basis.

The soil erodibility classification proposed by Hanson & Simon (2001) is based on both the critical shear stress and the erosion rate coefficient determined from JETs. The Hanson & Simon system recognizes five categories from very resistant to very erodible materials.

The second method proposed by Marot et al. (2011) is based on the energy dissipation between the fluid and the soil. The energy equation for the fluid (neglecting the soil phase inside the volume) can be written as:

$$\begin{aligned}\frac{dE}{dt} &= \frac{d}{dt}\iiint_{Mass}\left(e_{int} + \frac{u^2}{2} + \vec{g}.\vec{x}\right).dM \\ &= \frac{\partial}{\partial t}\iiint_{Volume}\left(e_{int} + \frac{u^2}{2} + \vec{g}.\vec{x}\right).\rho_W dV + \oiint_S\left(e_{int} + \frac{u^2}{2} + \vec{g}.\vec{x}\right).\rho_W.(\vec{U}.\vec{n}).dS\end{aligned} \tag{7}$$

where M: fluid mass, V: fluid volume, e_{int}: internal energy, S: interface between fluid and environment, n: normal vector of interface, U: fluid velocity (components: u, v, w), g: gravity, ρ_w: fluid density, x: coordinates.

Total energy is the sum of the mechanical work W and the energy exchange between the system and the environment E_{Ther}:

$$\frac{dE}{dt} = \frac{dE_{Ther}}{dt} + \frac{dW}{dt} \tag{8}$$

The whole experimental system is placed in a temperature controlled laboratory and it is supplied by the public water system. Thus for test duration, the system can be considered isothermal in time and internal energy is assumed constant. All tests are performed under the same experimental conditions, so the comparison of tests leads to neglect the relative variations of energy exchange between the system and the environment. In consequence the term dE_{Ther} / dt is negligible. As jet test results are analyzed in steady state (assuming during a time step that the water speed evolves slowly), the unsteady term of the kinetic energy is negligible. Finally the Equation 7 becomes:

$$\frac{dW}{dt} = \oiint_S\left(\frac{u^2}{2} + \vec{g}.\vec{x}\right)\rho_w\,(\vec{U}.\vec{n}).dS \tag{9}$$

The mechanical work W is the sum of: work done by pressure, viscous work in the fluid and work by erosion:

$$\frac{dW_{pressure}}{dt}+\frac{dW_{viscous\ in\ fluid}}{dt}+\frac{dW_{erosion}}{dt} = \iint_S \left(\frac{u^2}{2}+\vec{g}.\vec{x}\right).\rho_w.(\vec{U}.\vec{n}).dS \quad (10)$$

In comparison with free jet, a jet in front of a soil-water interface is subjected to a deviation from the centerline. It is assumed that the erosion is mainly associated with this deviation which induces an increase of shear stress and a great variation of pressure.

In front of a wall, Beltaos & Rajaratnam (1974) observed that wall shear stress increases linearly with lateral distance from jet centerline up to a maximum value obtained for r = 0.14 J and then decreases with any further increase in r. Moreover, when r/J ratio increases from 0 to 0.14, wall pressure decreases rapidly reaching 10% of maximum value of stagnation pressure on jet centerline axis. Thus at J depth, erosion energy is assumed to come from the space defined by lateral distance from jet centerline $r \leq 0.14$ J.

Beltaos & Rajaratnam (1974) proposed an expression of the vertical velocity on the jet axis:

$$\frac{u(r,Z)}{u(0,Z)} = \exp\left(-0.693\left(\frac{r}{b_u}\right)^2\right) \quad (11)$$

With the objective to take into account the variation of vertical velocity with the J altitude and with the distance r from the jet axe considered, Equations 10 and 11 are combined to express the temporal derivative of mechanical work through erosion by:

$$\frac{dW_{erosion}}{dt} = \pi \int_0^{0.14J} \rho_w\, u^3(0,J)\left(\exp\left(-0.693\left(\frac{r}{b_u}\right)^2\right)\right)^3 r\, dr \quad (12)$$

For convenience, the temporal derivative mechanical work by erosion is named erosion power ($P_{erosion}$).

The energy dissipated by erosion ($E_{erosion}$) is the time integration of the instantaneous erosion power for the test duration. Thus for each test, the erosion energy is computed by trapezoidal rule and the erosion resistance index is built with the erosion energy and the cumulative eroded dry mass (m_{dry}):

$$I_\alpha = -\log\left(\frac{m_{dry}}{E_{erosion}}\right) \quad (13)$$

Marot et al (2011) proposed six categories of soil erodibility: highly erodible for $I_\alpha < 1$, erodible for $1 \leq I_\alpha < 2$, moderately erodible for $2 \leq I_\alpha < 3$, moderately resistant for $3 \leq I_\alpha < 4$, resistant for $4 \leq I_\alpha < 5$ and highly resistant for $I_\alpha \geq 5$. By using the energy analysis, an identical erodibility classification of seven soils, covering a large range of erodibility, can be obtained with JET and Hole Erosion Test devices (Regazzoni & Marot 2013).

1.4 *Estimation of erosion resistance index from other soil properties*

Regazzoni & Marot (2012) determined the erodibility of twelve natural soil specimens which were compacted with the standard Proctor procedure at optimum water content less 1%. These soils represent a large range of erosion sensitivity. A wide dissipated hydraulic energy scale appears and a statistical analysis was carried out. By distinguishing the dispersive behavior from non-dispersive behavior, the multivariate statistical analysis leads to an expression of the erosion resistance index as a function of three physical parameters: compaction, saturation ratio and difference between clay water content and liquid limit.

These results revealed also that water content discrepancy of 4% is sufficient to induce a variation of soil erodibility from highly resistant to erodible. Then, even for specimens compacted with the standard Proctor procedure, soil erosion sensibility seems to depend on another key parameter which has to be studied.

This paper deals with the jet results analyzed by two interpretative methods and the relationship between interface erosion sensibility and other soil properties.

2 SOILS TESTED AND TESTING PROGRAM

2.1 *Properties of tested soils*

A series of tests was performed using clayey sands. Figure 2 shows the grain-size distribution of the used materials which were measured by a laser diffraction particle-size analyzer.

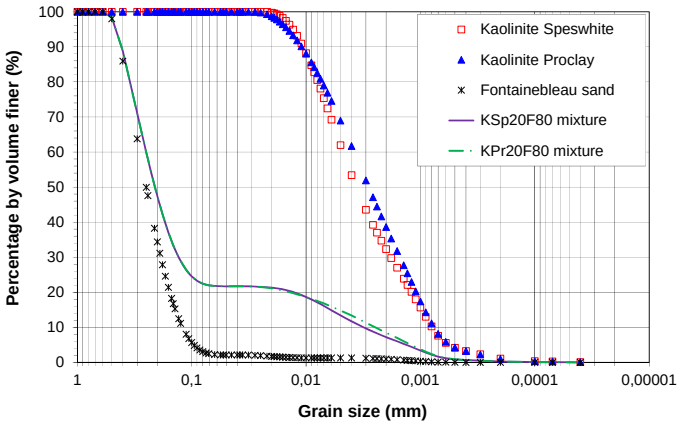

Figure 2. Grain size distribution of clays, sand and tested clayey sands.

Tests were performed on two mixtures of 20% kaolinite clay and 80% sand. The sand is a Fontainebleau sand (grain-size distribution within the range 0.4–600 µm, mean diameter D_{50} = 250 µm, uniformity coefficient of 2.38, and density of 26.5 kN/m^3). Two kaolinite clays were tested: the

first is referred as Speswhite (grain size distribution within the range 0.04–25 µm, D_{50} = 3.65 µm, uniformity coefficient of 6.04, and grain density of 25.5 kN/m^3). The second kaolinite clay (i.e., Proclay) has a slight different grain-size distribution (grain size distribution within the range 0.04–32 µm, D_{50} = 2.84 µm, uniformity coefficient of 5.03, and grain density of 25.7 kN/m^3).

Table 1 summarizes the chemical composition of materials (chemical analysis by X-ray fluorescence, provided by the supplier).

Table 1. Chemical composition of tested materials.

Mineralogy	Speswhite	Proclay	Fontainebleau sand
SiO_2 (%)	48.2	56.4	>99.7
Al_2O_3 (%)	36.9	28.7	<0.13
Fe_2O_3 (%)	0.68	1.4	<0.03
TiO_2 (%)	0.02	1.2	<0.03
CaO (%)	0.06	0.3	<0.03
MgO (%)	0.24	0.3	
K_20 (%)	1.59	0.8	<0.03
Na_2O (%)	0.12	0.1	

The specimen preparation phase was divided into two steps: production of the specimen and dynamic compaction.

The sand grains are first mixed with selected moisture content. Then, while mixing continues, powder clay is progressively added, and mixing is then carried on for an additional 10 min. The grain size distributions of the obtained clayey sands (named KSp20F80 and KPr20F80) are plotted in Figure 2.

After ensuring homogeneity of the grain-size distribution, the specimens were prepared by using a dynamic compaction technique (specimen made in three layers of 25 blows with a normal Proctor rammer and a Proctor mold).

For the saturation of some specimens, carbon dioxide was injected followed by the saturation phase which required approximately 24 hours.

As shown in Figure 3, for KSp20F80 mixture and KPr20F80 mixture, the value of Proctor optimum dry density is 19.31 kN/m^3 and 18.96 kN/m^3 respectively. The optimum water content is 10% for both clayey sands.

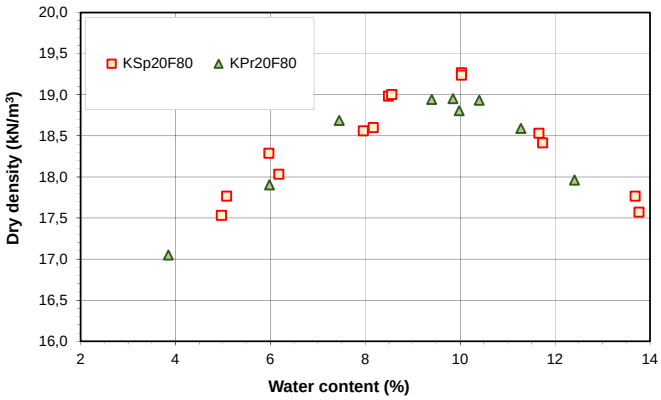

Figure 3. Dry density versus water content at compaction for tested clayey sands.

2.2 *Testing program*

For each performed tests, Table 2 indicates the type of clay present in the tested clayey sand (Speswhite, Sp or Proclay, Pr), the values of water content at compaction w, dry density γ_d, saturation ratio S_r and the applied hydraulic pressure P_a. Fourteen jet erosion tests were performed on KSp20F80 mixture specimens and nine tests were performed on specimens of KPr20F80 mixture.

Table 2. Main characteristics of performed jet erosion tests.

Nb test	Clay	w (%)	γ_d (kN/m^3)	S_r (%)	P_a (kPa)
1	Sp	4.97	17.53	27.49	8.4
2	Sp	5.08	17.77	91.41	16.9
3	Sp	5.97	18.29	37.86	8.4
4	Sp	6.18	18.03	95.70	8.4
5	Sp	7.96	18.56	53.15	8.4
6	Sp	8.17	18.60	98.56	8.5
7	Sp	8.49	18.98	61.52	8.4
8	Sp	8.56	19.00	91.22	8.4
9	Sp	10.03	19.27	76.93	7.1
10	Sp	10.03	19.24	80.97	8.5
11	Sp	11.74	18.41	76.25	8.4
12	Sp	11.66	18.53	77.43	8.4
13	Sp	13.77	17.57	76.69	8.4
14	Sp	13.69	17.77	78.95	8.4
15	Pr	3.85	17.05	97.99	8.5
16	Pr	5.98	17.90	35.23	8.5
17	Pr	7.45	18.69	50.78	8.4
18	Pr	9.40	18.94	67.35	8.4
19	Pr	9.85	18.95	70.67	8.4
20	Pr	10.40	18.93	74.33	8.4
21	Pr	9.98	18.81	94.19	8.5
22	Pr	11.28	18.59	75.46	8.5
23	Pr	12.41	17.96	73.92	8.4

3 TEST RESULTS

3.1 *Results of JET analysis by Hanson & Simon's method*

The results of jet erosion tests are first analyzed thanks to the Hanson & Simon's method and they are plotted in the corresponding soil erodibility chart (i.e. erosion coefficient versus critical hydraulic shear stress).

Figure 4 shows the results obtained for specimens of both clayey sand types which were compacted at the dry side of optimum. Only one specimen is erodible (Pr-16) all the others can be described as very erodible.

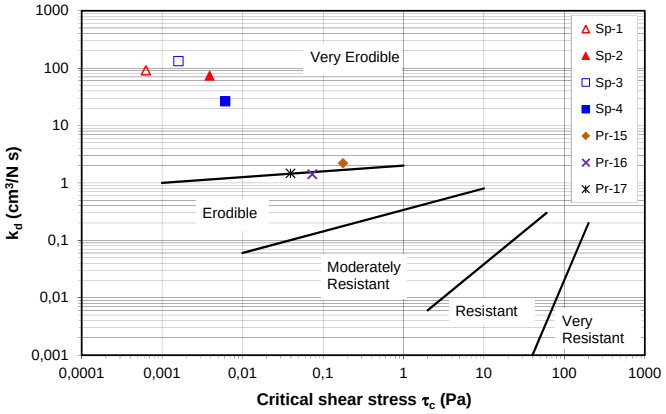

Figure 4. Erosion coefficient versus critical hydraulic shear stress (dry side, both clayey sands).

The Figure 5 shows the results of KSp20F80 specimens compacted at the optimum Proctor or at the wet side.

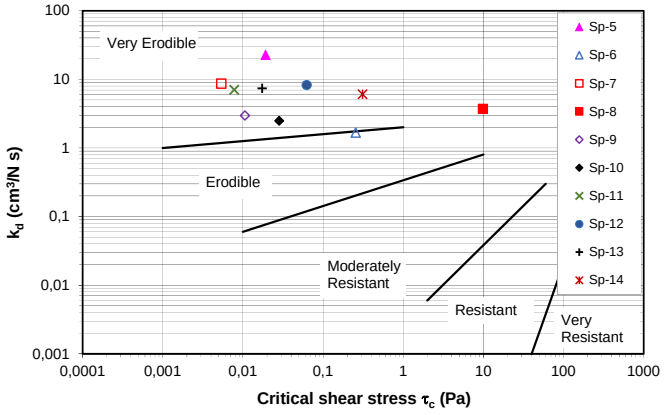

Figure 5. Erosion coefficient versus critical hydraulic shear stress (optimum and wet side, KSp20F80).

Among these specimens, only one is erodible (Sp-6), all the others are very erodible.

For specimens of KPr20F80 mixture compacted at optimum or at wet side (see Figure 6), four specimens can be described as erodible (Pr-18, Pr-19, Pr-20 and Pr-21) and two very erodible (Pr-22 and Pr-23).

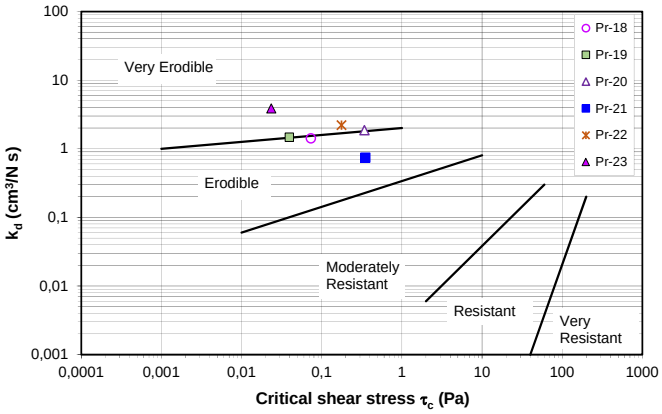

Figure 6. Erosion coefficient versus critical hydraulic shear stress (optimum and wet side, KPr20F80).

3.2 *Results of JET analysis by energy based method*

With the objective to take into account the history of the hydraulic loading on one hand, and the evolution of the corresponding specimen answer on the other hand, the cumulative eroded mass is plotted versus the cumulative expended energy. Such chart can be divided in several areas according to the value of the ratio $m_{\text{eroded dry mass}} / E_{\text{erosion}}$, related to the erodibility classification which is defined by the value of the erosion rate index (Marot et al 2011).

Figure 7 shows the results of the energy analysis of tests performed with specimens of both clayey sands compacted at dry side of optimum.

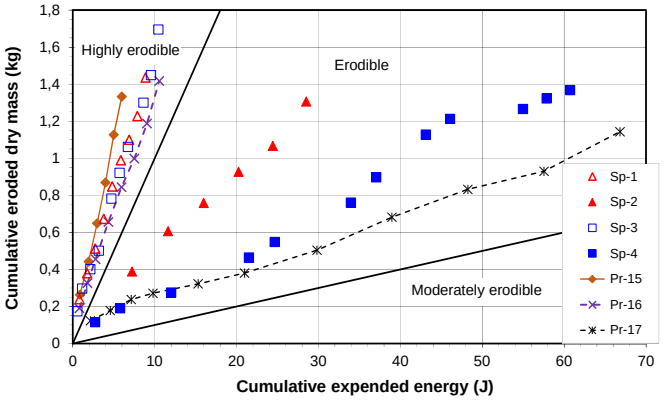

Figure 7. Cumulative eroded dry mass versus cumulative expended energy (dry side, both clayey sands).

According to this interpretative method, 4 specimens can be described as highly erodible (Sp-1, Sp-3, Pr-15 and Pr-17) and three specimens as erodible (Sp-2, Sp-4 and Pr-17).

As shown in Figure 8, among specimens of KSp20F80 compacted at optimum or at wet side of optimum, 2 specimens are erodible (Sp-5, Sp-2) and the others are moderately erodible (Sp-6, Sp-8, Sp-9, Sp-10, Sp-11, Sp-12, Sp-13 and Sp-14).

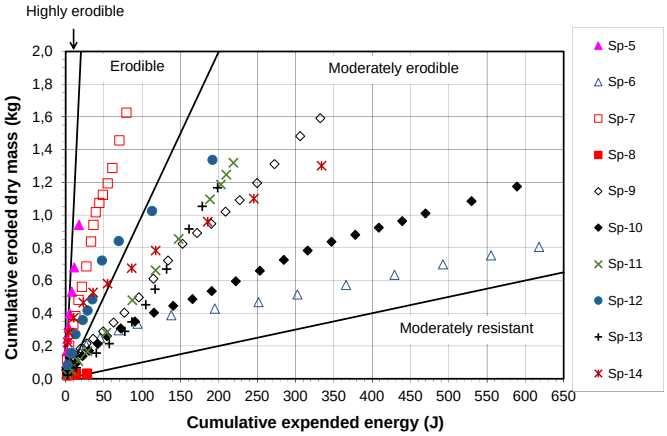

Figure 8. Cumulative eroded dry mass versus cumulative expended energy (optimum and wet side, KSp20F80).

For specimens of KPr20F80 mixture compacted at optimum or wet side, classification of specimen Pr-21 is moderately resistant (see Figure 9) and others specimens are classified moderately erodible (Pr-18, Pr-19, Pr-20, Pr-22 and Pr-23).

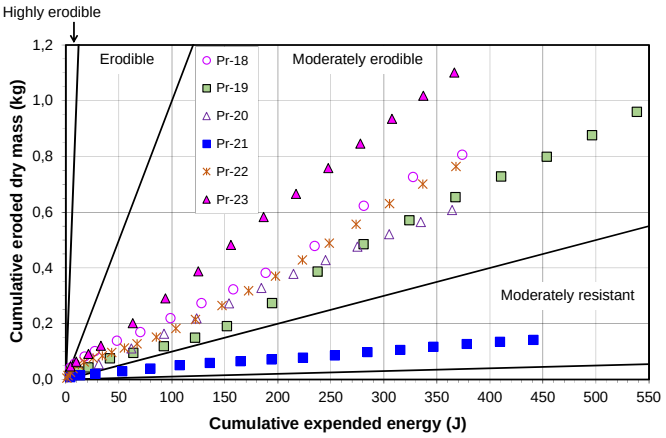

Figure 9. Cumulative eroded dry mass versus cumulative expended energy (optimum and wet side, KPr20F80).

4 DISCUSSION

4.1 *Comparison between erodibility classifications*

The comparison of results obtained thanks to both interpretative methods is shown in Table 3.

All specimens appear relatively erodible with both methods and specimen Pr-21 is the most resistant.

However, with Hanson & Simon's method, 17 specimens are classified very erodible and 6 erodible (Sp-6, Pr-16, Pr-18, Pr-19, Pr-20 and Pr-21), whereas energy based method gives: 4 specimens highly erodible (Sp-1, Sp-3, Pr-15 and Pr-16) and 5 specimens erodible (Sp-2, Sp-4, Sp-5, Sp-7 and Pr-17).

Fourteen specimens classified very erodible by Hanson & Simon's method are described as erodible or moderately erodible by energy based method (Sp-2, Sp-4, Sp-5, Sp-7, Sp-8, Sp-9, Sp-10, Sp-11, Sp-12, Sp-13, Sp-14, Pr-17, Pr-22 and Pr-23).

Table 3. Comparison of erodibility classifications.

Nb test	k_d (cm^3/N.s)	τ_c (Pa)	I_α	[a]Class.	[b]Class.
1	91.55	0.0006	0.84	Very erodible	Highly erodible
2	73.91	0.0039	1.38	Very erodible	Erodible
3	132.40	0.0016	0.83	Very erodible	Highly erodible
4	26.39	0.0061	1.64	Very erodible	Erodible
5	22.73	0.0192	1.33	Very erodible	Erodible
6	1.68	0.2557	2.89	Erodible	Moderately erodible
7	8.64	0.0054	1.70	Very erodible	Erodible
8	3.71	9.8820	2.96	Very erodible	Moderately erodible
9	2.97	0.0106	2.34	Very erodible	Moderately erodible
10	2.49	0.0284	2.70	Very erodible	Moderately erodible
11	7.03	0.0078	2.22	Very erodible	Moderately erodible
12	8.25	0.0625	2.16	Very erodible	Moderately erodible
13	7.37	0.0174	2.23	Very erodible	Moderately erodible
14	6.04	0.3105	2.41	Very erodible	Moderately erodible
15	269.80	0.0290	0.65	Very erodible	Highly erodible
16	83.35	0.0010	0.87	Erodible	Highly erodible
17	7.17	0.0392	1.77	Very erodible	Erodible
18	1.41	0.0736	2.67	Erodible	Moderately erodible
19	1.47	0.0394	2.75	Erodible	Moderately erodible
20	1.86	0.3411	2.78	Erodible	Moderately erodible
21	0.74	0.3514	3.49	Erodible	Moderately resistant
22	2.21	0.1769	2.68	Very erodible	Moderately erodible
23	3.87	0.0235	2.52	Very erodible	Moderately erodible

[a]Classification according to Hanson & Simon (2001) soil erodibility system.
[b]Classification according to Marot et al. (2011) soil erodibility system.

Thus Hanson & Simon's method appears more conservative than energy based method and it seems to be easier to evaluate with the energy based method, the relative classification between different soils all described as very erodible by Hanson & Simon's method.

4.2 *Influence of density and saturation ratio*

By distinguishing the dispersive behavior from non-dispersive behavior, Regazzoni & Marot (2011) proposed an expression of the erosion resistance index as a function of three physical parameters: compaction, saturation ratio and difference between clay water content and liquid limit. However all tested specimens were compacted with the standard Proctor procedure at optimum water content less 1%. Thus for a given soil, it seems to be interesting to investigate the variations of erosion sensibility induced by the variation of water content at compaction.

According to the value of water content, the use of dynamic compaction technique permits to obtain several specimens characterized by a large range of values of saturation ratio and density. Moreover after compaction step, nine specimens were saturated (Sp-2, Sp-4, Sp-6, Sp-8, Sp-10, Sp-12, Sp-14, Pr-15 and Pr-21).

The values of erosion rate index versus saturation ratio are plotted in Figure 10 for specimens of KSp20F80 mixture and in Figure 11 for specimens of KPr20F80 mixture. For both clayey sands, specimens are distinguished according to the water content at compaction in comparison with optimum water content: dry side, optimum or wet side.

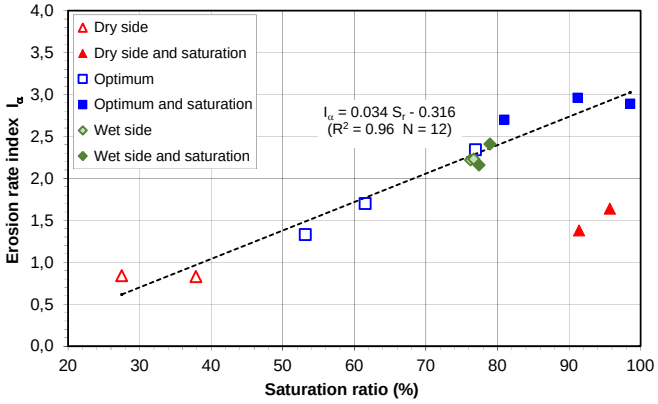

Figure 10. Erosion rate index versus saturation ratio (KSp20F80).

For both clayey sands and by considering all specimens, except specimens saturated after compaction at dry side (Sp-2, Sp-4 and Pr-15) a linear correlation can be expressed between erosion resistance index and saturation ratio. The obtained correlation coefficient (R^2) is 0.96, with a sample size N = 12 for KSp20F80 mixture and N = 8 for KPr20F80 mixture. Thus these results point out the great influence of saturation ratio on soil erodibility.

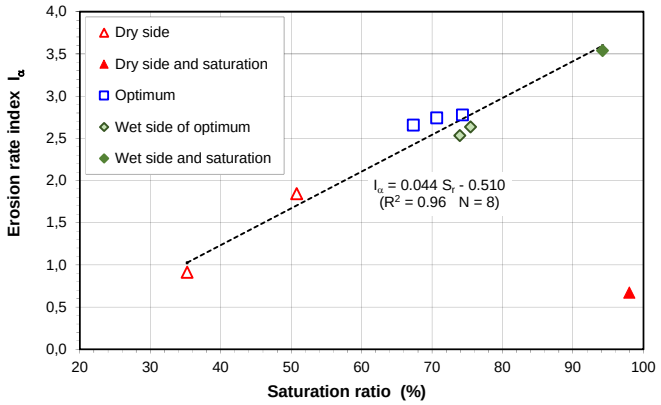

Figure 11. Erosion rate index versus saturation ratio (KPr20F80).

4.3 *Influence of soil micro fabric*

Let us now consider specimen Sp-2, saturated after compaction at dry side and specimen Sp-14 saturated after compaction at wet side. Both specimens have the same dry density (17.7 kN/m^3) but Sp-2 is characterized by a value of saturation ratio $S_r = 91.41$ % and a value of erosion rate index $I_\alpha = 1.38$; whereas for Sp-14 $S_r = 78.95$ % and $I_\alpha = 2.41$. Moreover the comparison of specimens compacted at dry side with specimens compacted at wet side shows that the corresponding values of erosion rate index are systematically smaller at dry side. In consequence, these results reveal that even after saturation, specimens compacted at dry side stay more erodible than specimens compacted at wet side.

With the aim to study the micro fabric of tested soils, for each clayey sand three specimens were prepared by dynamic compaction technique (normal Proctor protocol) with three different values of water content corresponding with the optimum, dry or wet side. A sample was extracted in each specimen in order to be dried during 24 hours at 60°C. Then mercury injection porosimetry (MIP) measurements were performed with Micromeritics porosimeter (Autopore III 9420) whose range of pressure reaches more than 200 MPa. This pressure allows the mercury to penetrate pores of 6nm of diameter approximately, according to Whasburn's law.

The pore size distribution is plotted in Figure 12 for KSp20F80 mixture and in Figure 13 for KPr20F80 mixture. For both clayey sands, the range of pore size distribution is between 6 nm and 10,000 nm. The percolation diameter can be defined as the pore diameter corresponding with the maximum value of mercury injection.

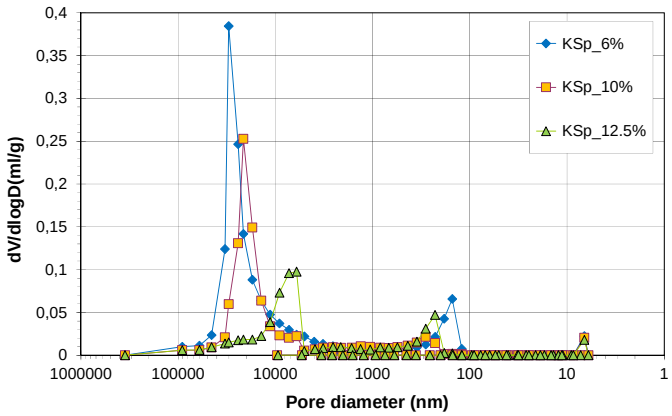

Figure 12. Pore size distribution (KSp20F80).

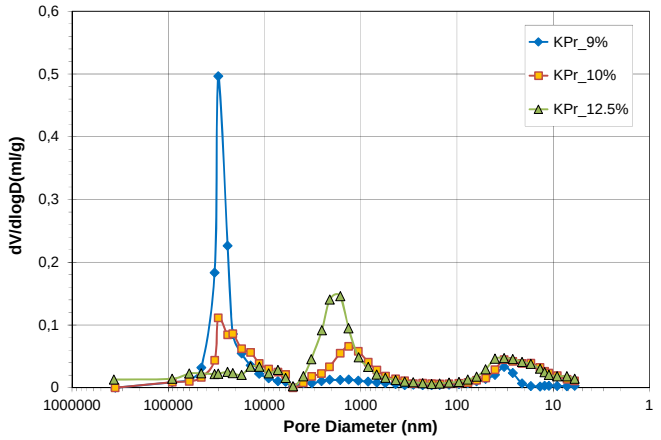

Figure 13. Pore size distribution (KPr20F80).

As shown in Table 4, the value of percolation diameter decreases from dry side to optimum and wet side.

Table 4. Main characteristics of MIP tests.

Type of clay	Water content at compaction (%)	Percolation Diameter (nm)
Sp	6	30189
Sp	10	21314
Sp	12.5	6637
Pr	9	30192
Pr	10	30188
Pr	12.5	1863

The results quoted above underline that the interface erosion sensibility decreases with the percolation diameter and this diameter appears appropriate for characterizing the influence of soil micro fabric. Further studies are required to confirm the influence of micro fabric of soils covering a large range of interface erosion sensibility.

5 CONCLUSION

A Jet Erosion Test device was used in order to characterize the sensitivity to interface erosion of two types of clayey sand. Twenty-three specimens were compacted (according to normal Proctor procedure) with different water contents and some specimens were also saturated after compaction step.

Jet erosion test results were analyzed by two interpretative methods and the comparative study reveals that energy based method is less conservative and appears more efficient in order to elaborate a relative classification of erodible soils.

For both tested clayey sands, the erosion sensibility, defined by the erosion resistance index is linearly related with the saturation ratio. However, even after saturation, specimens compacted at dry side stay more erodible than specimens compacted at wet side. These results reveal the influence on interface erosion sensibility of soil micro fabric that can be characterized by percolation diameter of mercury injection.

6 ACKNOWLEDGMENTS

The authors thank the World Bank (Project TRIG, University of Danang, Vietnam), Electricité De France, the French National Research Agency (ANR-ERINOH) and the French Institute for Applied Research and Experimentation in Civil Engineering (IREX) for providing financial support for this work.

7 REFERENCES

ASTM. 2000. Standard test method for erodibility determination of soil in the field or in the laboratory by the jet index method. *Geotechnical engineering standards.* D5852.

Beltaos, S. & Rajaratnam, N. 1974. Impinging circular turbulent jets. *Journal of the Hydraulics Division*, HY10: 1313-1328.

Blaisdell, F.W. & Anderson, C.L. 1981. Ultimate dimension of local scour. *Journal of Hydraulics Division, ASCE* 107(HY3): 327-337.

Dunn, I.S. 1959. Tractive resistance of cohesive channels. *Journal of Soil Mechanics and Foundation Division, ASCE* 85(SM3): 1-24.

Fell, R. & Fry, J.J. 2007. *Internal erosion of dams and their foundations*, Editors, Taylor & Francis Publisher.

Hanson, G.J & Simon, A. 2001. Erodibility of cohesive streambeds in the loess area of the Midwestern USA. *Hydrological Processes* 15(1): 23-38.

Hanson, G. J. & Cook, K. R. 2004. Apparatus, Tests procedures, and analytical methods to measure soil erodibility in-situ. *Applied Engineering in Agriculture* 20(4): 455-462.

Marot, D., Regazzoni, P.L., Wahl, T. 2011. Energy based method for providing soil surface erodibility rankings. *Journal of Geotechnical and Geoenvironmental Engineering, ASCE* 137(12): 1290 – 1294.

Regazzoni, P.L. & Marot, D. 2011. Investigation of interface erosion rate by Jet Erosion Test and statistical analysis. *European Journal of Environmental and Civil Engineering* 15(8): 1167-1185.

Regazzoni, P.L. & Marot, D. 2013. A comparative analysis of interface erosion tests. *Natural Hazards* 67(2): 937-950.